COBEM 2021 26th International Congress of Mechanical Engineering
November 22-26, 2021, Virtual Congress, Brazil

Validation and Analysis of Turbulence Modeling in Secondary Flow Conditions using OpenFOAM

Ana Cristina Neves Carloni
Universidade Estadual Paulista - UNESP, Faculdade de Engenharia, Departamento de Engenharia Mecânica, 15385-000, Ilha Solteira, SP, Brasil
ana.carloni@unesp.br
Kevin Eduardo de Conde
Instituto Tecnológico de Aeronáutica, 12228-900, São José dos Campos, SP, Brasil
kevin@ita.br
Aluisio Viais Pantaleão
Universidade Estadual Paulista - UNESP, Faculdade de Engenharia, Departamento de Engenharia Mecânica, 15385-000, Ilha Solteira, SP, Brasil
aluisio.pantaleao@unesp.br

Abstract. *The present work proposes to analyze five RANS turbulence models' performance in predicting an internal single-phase incompressible turbulent flow through an elbow pipe using OpenFOAM. Validation is achieved by the comparison with LES and experimental benchmark results. Additionally, such results are used to compare among turbulence models and to determine the most adequate one in terms of accuracy envisioning further application in multiphase flows. Results show that the $k-\omega$ SST is the most appropriate turbulence model to predict the velocity profile in regions of significant streamline curvature, whereas in the presence of high adverse pressure gradient the most appropriate one is the realizable $k-\epsilon$. Furthermore, a quantitative analysis suggests that a modification to the F_1 blending function in the $k-\omega$ SST model may improve the velocity agreement with LES benchmark results by postponing the transition to the $k-\epsilon$ formulation in the model. Results suggest that the unsteadiness of turbulence may be as relevant as the anisotropic characteristics in describing the flow dynamic.*
Keywords: *Turbulence models, Secondary-flow, 90-degree bent elbow, Pipe bend*

1. INTRODUCTION

Scientific interest resides in understanding turbulent phenomena in order to provide knowledge applicable to various configurations of interest. Despite extensive scientific investigation, turbulence has been designated the major unsolved problem in classical physics (Wilcox *et al.*, 1998). When applying the Reynolds-averaging to the governing equations of fluid dynamics, the main difficulty encountered is the closure problem of the Navier-Stokes equations, which nonlinearities lead to the appearance of the unknown term called the Reynolds stress tensor. This has motivated the development of turbulence modeling to provide approximations for the unknown correlations related to the flow's known properties, in order to equate the number of equations to the number of unknown terms and, therefore, enabling the solution of the system of equations.

Over the last decades turbulence models have been analyzed and their validation in different applications and geometries are continuously investigated (Oberkampf and Trucano, 2002). For instance, Kim *et al.* (2014) evaluated eleven turbulence models by comparing them with experimental data from Sudo *et al.* (1998), and established quantitative criteria for selecting the turbulence model that most closely describes the velocity profile at the outlet of a pipe elbow. Focusing on the development of geometry-induced secondary flows for Dean numbers greater than 20700, the analysis of the turbulence models was restricted when investigating them exclusively in the region prior to recirculation. Among the models that satisfy the established criteria are the realizable $k-\epsilon$, RNG $k-\epsilon$, and $k-\omega$ SST. Similarly, Röhrig *et al.* (2015) evaluate the performance of LES (Large-Eddy Simulation), RSM (Reynolds Stress Model) and of a RANS (Reynolds-Averaged Navier-Stokes) model corresponding to the standard k-ϵ at a 90-degree elbow pipe, a condition in which the streamlines exhibit significant curvature and there are potential flow detachments. This system corresponds to an incompressible turbulent internal flow in a 90-degree elbow pipe for Dean numbers of nearly 13500 and 19000.

Nevertheless, instead of the perspective of determining a unique and universally accurate turbulence model, researchers recognize that there is still a prominent demand to improve RANS models and also to determine optimized application-oriented turbulence models (Duraisamy *et al.*, 2017). Aware of this widely experienced constraint, this paper proposes to analyze the performance of RANS turbulence models on a geometry with challenging phenomena in terms of turbulence modeling, with the aim of determining the most appropriate turbulence model among the proposed ones. More specifically, it was analyzed a single-phase turbulent incompressible internal flow in a 90-degree pipe with a circular cross section,

for further application in multiphase flow. Thus, the establishment of an appropriate RANS turbulence model is based on the criteria of reproducing the flow velocity field of LES and experimental benchmark results accurately, since the main effect on interaction between the continuous and the dispersed in the context of multiphase flows is given as a function of the friction velocity (Sommerfeld and Laín, 2012).

2. TURBULENCE MODELING CHALLENGES

The elbow geometry was selected because it is both simple and sufficiently representative in terms of turbulence modeling challeging phenomena. Such representativeness is guaranteed either by the flow's characteristics, as well as by the presence of physical phenomena that occur in general applications. Among the phenomena that are worth mentioning are the geometry-induced favorable and adverse pressure gradients, streamlines curvature, velocity profile's heterogeneities, and the development of secondary flows related to the transverse movement of streamlines. It is of particular interest to verify the presence of boundary layer detachment points along the flow, which are not previously known. In other words, depending on the geometry and boundary conditions, the flow can detach from the pipe surface or remain attached. The presence of geometry-induced favorable and adverse pressure gradients are caused by the curvature of the streamlines in the elbow region. These pressure gradients are responsible for boundary layer detachment, which directly affects performance parameters such as pressure drop and drag coefficient (White and Corfield, 2006; Crawford *et al.*, 2009).

Another phenomenon found in this geometry is the development of secondary flow. Caused by the imbalance between the centrifugal force and the near-wall pressure gradient at the pipe bend, the secondary flow consists in a pair of counter-rotating cells that propagate longitudinally, designated Dean vortices. It is known that the secondary flow overlaps the primary flow within the duct, and therefore alters the flow dynamics (Bradshaw, 1987; Larsson *et al.*, 2011). Dean vortices are characteristic of flows in elbows, bent pipes, and canals. In these cases, the adverse pressure gradient is responsible for the appearance of secondary flow as the fluid in the center of the pipe moves to the outer wall of the elbow, while the fluid in the inner wall moves towards its center. It is important to point out that the Dean number contributes to the assurance of dynamic similarity between the present and the literature works, which provides reference experimental and LES data.

3. EDDY-VISCOSITY TURBULENCE MODELS

It is important to remember that the system of equations composed by the mass, linear momentum, and energy conservation equations are not directly solved, due to the significant computational cost involved (Pope, 2001). As an alternative, the application of Reynolds averaging expresses these equations as a function of known average variables, fostering the solution. However, the appearance of the unknown Reynolds stress tensor causes the closure problem, which consists of the impossibility of equating the number of equations to the number of unknown terms. Hence, the Boussinesq approximation models the Reynolds stress tensor similarly to the dissipative term already found in the Navier-Stokes equations, however, described as a function of the turbulent viscosity (Davidson, 2015; Pope, 2001).

Therefore, the solution of the governing equation no longer depends on the computation of the Reynolds stress tensor, but of the turbulent viscosity. For this reason, turbulence models propose different approaches to determine the turbulent viscosity and, consequently, enable the solution of the equations (Wilcox *et al.*, 1998; Davidson, 2015). In the present work, the performance of five RANS turbulence models were evaluated when addressing challenging phenomena from the perspective of turbulence modeling. These models correspond to the $k-\omega$ SST, standard $k-\epsilon$, realizable $k-\epsilon$, RNG $k-\epsilon$, and the Shih's nonlinear $k-\epsilon$ model.

3.1 Standard $k-\epsilon$

The standard $k-\epsilon$ turbulence model solves transport equations for two turbulence parameters - the turbulent kinetic energy k and the turbulence dissipation rate ϵ. The application of these transport equations aims to address the dissipative aspect of turbulence by considering the turbulence history from a deterministic standpoint. It is implemented in OpenFOAM the standard $k-\epsilon$ model based on the work of Launder and Spalding (1974). The standard $k-\epsilon$ turbulence model has satisfactory accuracy for a wide range of applications, especially in external flows (Breunig, 2017). In general, it is reported that this turbulence model has low accuracy in predicting flows with boundary layer detachment, significant streamline curvature and adverse pressure gradients (Jones and Launder, 1972). In particular, it is well known that the standard $k-\epsilon$ turbulence model is not able to provide accurate results for flows with high shear rates or significant boundary layer detachment. Furthermore, the transport equation for the turbulent kinetic energy dissipation rate ϵ does not always provide the appropriate length scale for the turbulence that occurs in the flow. In these cases, the turbulent viscosity is overestimated by assuming its standard formulation (Shih *et al.*, 1994).

3.2 Realizable $k-\epsilon$

The realizable $k-\epsilon$ turbulence model was proposed in order to improve the standard $k-\epsilon$ model's performance, as the latter overestimates the turbulent viscosity in flows with high mean strain rate or significant flow detachment. To address these performance limitations, the realizable $k-\epsilon$ turbulence model proposed formulations for the transport equation of the turbulence dissipation rate ϵ and also for the turbulent viscosity. The first proposed improvement is intended to provide a more representative, simple and robust model, where the realizable $k-\epsilon$ transport equation differs from the standard $k-\epsilon$ turbulence model in the production term.

The second improvement intends to ensure that the turbulent viscosity formulation is realizable, which is not always the case in standard $k-\epsilon$ model formulation, since normal stresses can assume negative values, thus disrespecting Schwarz's inequality for shear stresses. The applied modifications result mainly in improvements in the prediction of flow in complex structures, as well as flow involving rotation, boundary layers with significant adverse pressure gradients, streamline curvature, flow detachment and recirculation. The realizable $k-\epsilon$ turbulence model implemented in OpenFOAM is based on the work of Shih *et al.* (1994).

3.3 RNG $k-\epsilon$

Depending on the application, the Reynolds-averaging procedure can mitigate relevant turbulence features of the flow. The dissipative term $\mathcal{R}$, derived from the application of the RNG method, considers anisotropic effects of the turbulence, while maintaining the use of the Boussinesq hypothesis for the Reynolds stress tensor (Perini *et al.*, 2017). By comparison, the standard $k-\epsilon$ turbulence model does not compute the additional term $\mathcal{R}$, analogous to the Reynolds stress tensor, because it assumes isotropy locally. The implementation of the RNG turbulence $k-\epsilon$ model in OpenFOAM is based on the work of Yakhot *et al.* (1992). The proposed RNG $k-\epsilon$ model provides accurate results in applications with simple shear stresses, since the ϵ transport equation does not consider the effects of rotating stresses. These rotational effects may be relevant in turbulent flows with streamline curvature (Yakhot *et al.*, 1992). Furthermore, the RNG $k-\epsilon$ model underestimates the value of the turbulent kinetic energy k, implying less dissipative and more realistic flows when applied to complex geometries (Breunig, 2017).

3.4 $k-\omega$ SST

The $k-\omega$ SST turbulence model was developed from the combination of the $k-\epsilon$ and $k-\omega$ models in order to eliminate their particular limitations. Since the $k-\epsilon$ model is not sensitive to the initial and boundary conditions of the flow, the $k-\omega$ SST turbulence model aims to apply the $k-\omega$ model near the walls and then to transition to the $k-\epsilon$ model as it moves outward from the wall (Menter, 1992). To switch between both models, the blending function F_1 is included, where $F_1 = 0$ results in the $k-\epsilon$ model, while $F_1 = 1$ corresponds to the turbulence model $k-\omega$. In addition to the F_1 blending function, the $k-\omega$ SST model, based on the work of Menter *et al.* (2003), includes a viscosity limiter. The turbulent viscosity limitation occurs with increasing blending function F_2 which, in turn, is dependent on the distance to the wall. This factor is mainly responsible for yielding results close to experimental data with moderate flow detachment (Menter *et al.*, 2003).

3.5 Shih's nonlinear $k-\epsilon$

Based on the standard $k-\epsilon$ model, Shih's nonlinear $k-\epsilon$ turbulence model was developed to provide the Reynolds stress tensor based on a general algebraic expression and the concept of realizability. This turbulence model is implemented in OpenFOAM based on the work of Shih (1993), in which the turbulent constitutive relation that relates the Reynolds stresses to the mean velocity gradients is truncated up to its tensorial quadratic terms. In comparison, classical isotropic eddy viscosity models approximate this turbulent constitutive relation linearly. The proposed formulation of Shih's $k-\epsilon$ model exhibits significant improvement in performance compared to the standard $k-\epsilon$ turbulence model in rotating flows and with skewness (Shih, 1993). However, the constitutive relation arising from the application of invariance theory is valid only for turbulent flows with high Reynolds numbers, as the influence of viscosity is not considered in the analysis.

4. METHODOLOGY

4.1 Geometry Description

The investigations were carried out in a circular transverse section duct of diameter D with curvature of 90^o, whose radius of curvature corresponds to $R_c = 1.58D$, as depicted in Fig. 1(a). Prior and posterior to the curvature, the geometry is composed of rectilinear ducts of length $4.31D$ and $4.43D$, respectively. In addition, the angular ϕ and linear z coordinates were determined in order to specify sectional planes perpendicular to the pipe centerline. On the other hand,

the r' coordinate is specified in the corresponding plane and varies between $0 \leq r' \leq R$, where R is the radius of the duct. Such parameters were based on the work of Röhrig *et al.* (2015), used as a benchmark due to disposing of LES data and comparing them with experimental data of Kalpakli and Örlü (2013) in the aforementioned geometry.

4.2 Computational Grid

In computational fluid dynamics, physically meaningful results can be accomplished from the solution of a system of algebraic equations. These equations result from the discretization of the mathematical model over a computational grid. Grid determination must be oriented towards minimizing the error in the solution (Moukalled *et al.*, 2016; Conde, 2018). In turbulence modeling, an important aspect is the establishment of the mesh dimensionless wall variable y^+, which corresponds to a dimensionless measurement of the distance between the nearest wall and the adjacent mesh element cell center. It is recommended to set y^+ between 30 and 200 when using wall functions associated with turbulence models, such as the standard $k - \epsilon$ (Bredberg, 2000). In this y^+ range the wall function is used to model the boundary layer behaviour in both viscous and buffer layer, whereas the turbulence model solves exclusively the logarithmic layer. On the other hand, it is recommended to set $y^+ \sim 1$ when using a wall-resolved turbulence model.

Grid independence analysis was performed by generating three meshes with different refinements, which are $y^+ = 60$, $y^+ = 30$ and $y^+ = 0.9$. Comparing their results in similar conditions, it was observed that the results using $y^+ = 30$ and $y^+ = 0.9$ revealed no discrepancies. The grid-independent wall functions implemented in OpenFOAM allow for the use of wall-resolved meshes in combination with models which require wall-functions. For those reasons, the computational mesh resolution with $y^+ = 0.9$ was established for all turbulence models investigated herein to compare their performance under similar conditions. Additionally, the $y^+ \sim 1$ condition is also in agreement with similar-scope works of Röhrig *et al.* (2015) and Kim *et al.* (2014). The resulting mesh depicted in Fig. 1(b) contains 755445 elements, which are majorly composed of hexahedrons.

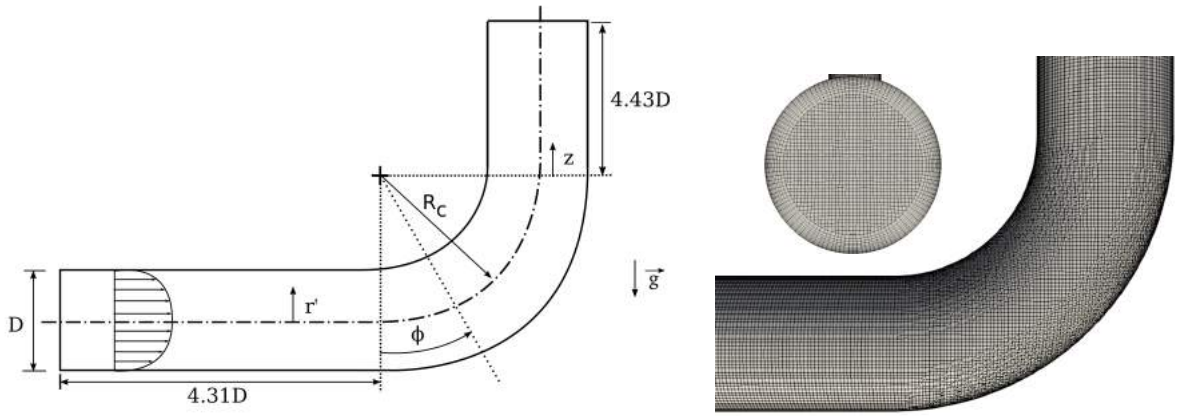

(a) (b)

Figure 1. (a) Schematic diagram at the symmetry plane of the elbow specifying geometrical parameters and the described coordinates. (b) Computational grid for the presently considered geometry in the outer wall of the pipe bend and its cross-section; the latter view being enlarged for the sake of clarity.

4.3 Boundary Conditions

The solution of a partial differential equation requires the definition of boundary conditions to be applied to the domain contours. Specifically for the turbulent parameters k, ϵ, ω and ν_t, wall functions were used. In essence, wall functions are empirical functions fitted to the observed behaviour described by the law of the wall in order to predict the same wall shear stress as the wall-resolved linear approach (Bredberg, 2000; Fox *et al.*, 2020). The wall functions used in this case apply a discontinuous (stepwise) function in the respective variable computation whereby the switch between equations is based on the estimated intersection of the viscous and inertial sublayers. Such grid independent approach allows the comparison of both wall-resolved and wall-modeled turbulence models in the same grid.

A fully developed velocity profile was used as inlet boundary condition. For the velocity, it has been accomplished by estimating the fully developed velocity profile using the empirical power-law with exponent $n = 6.36$ (Fox *et al.*, 2020). Corresponding boundary conditions for the turbulent parameters were established according to the implemented fully developed velocity profile at the inlet. At outlet, a zero gradient boundary condition in case of reverse flow combined to a fixed magnitude was used for the ϵ and ω. At the pipe wall, the flow velocity was established with a no-slip condition, while the boundary conditions for k, ω and the turbulent viscosity ν_t were defined using wall functions in a grid-independent manner (Greenshields, 2020).

At outlet, the applied boundary condition determines the velocity based on the flow normal to the surface direction in case of reverse flow. In addition, it sets zero gradient to flow outside the domain, i.e., it considers that the velocity at the duct's exit becomes fixed once outside the domain. It is interesting to note that when determining zero gradient, this boundary condition may influence the analysis of the flow after the bend. For this reason, longer lengths of straight duct after curvature are considered when focusing on phenomena in this region. In comparison, the present paper considers the length of the rectilinear duct posterior to the bend equivalent to $4.43D$, whereas Kim *et al.* (2014) considers the length of $50D$ in order to analyze the Dean vortices' dynamic. Finally, corresponding zero gradient boundary conditions for the k, ϵ and ω have been applied, whereas μ_t is calculated from the previous variables.

5. RESULTS

5.1 Setup Validation

The considered benchmark results from Röhrig *et al.* (2015) correspond to the application of LES and the standard $k-\epsilon$ turbulence model, whose implementation is not specified. Aware of the differences between the implementations in the present work and also the RANS turbulence models' limitations, it is expected that the results will differ with regard to the benchmark. Thus, in order to ensure that the divergences are only from the characteristics of the turbulence models, it is necessary to verify that the setup was performed properly. For this purpose, setup validation was performed using semi-empirical expressions, such as the logarithmic law, in valid regions.

Initially, the flow prior to the bend was analyzed in two manners. The first one was to compare the velocity profiles normalized by the bulk velocity U_b at the plane of symmetry at 85% of the straight inlet length, as depicted in Fig. 2(a). In general, it is clear that the velocity profiles prior to the curvature are fully developed and therefore consistent with the established configuration. The second way to verify the computational simulation setup is to investigate whether the velocity profile behaves according to the logarithmic law in the straight section of the pipe. It is worth noting that, in contrast to the result in Fig. 2(a), the interest consists in the near-wall region. Located at 85% of the straight inlet pipe, i.e., prior to the curvature, Fig. 2(b) presents the velocity profiles departing from the wall for the investigated turbulence models, compared to the logarithmic law.

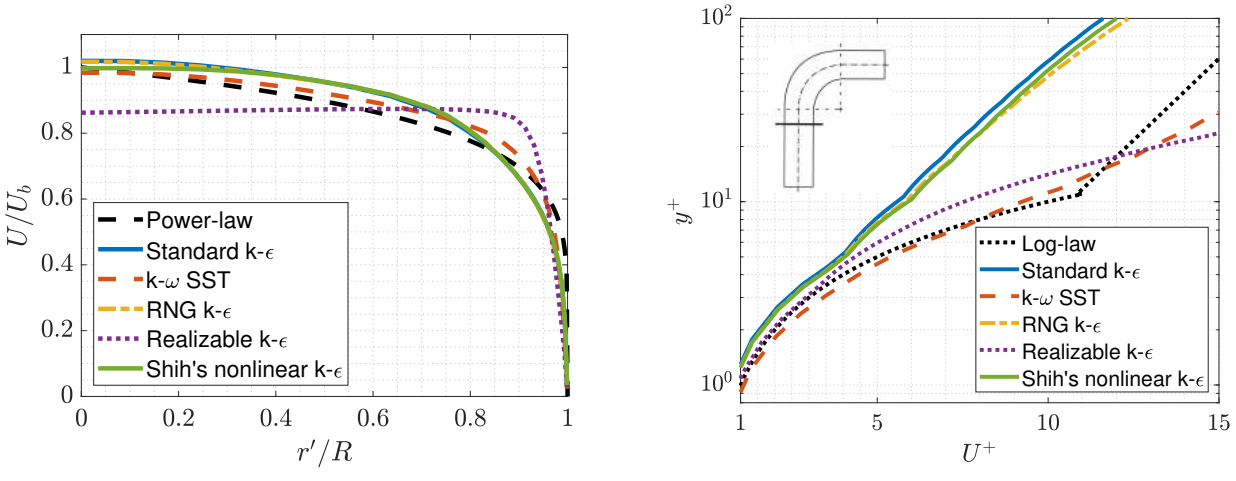

(a) (b)

Figure 2. (a) Velocity profile versus the power-law and (b) turbulent velocity profile versus the logarithmic law for the proposed turbulence models, both at 85% of the straight pipe length before curvature.

It can be observed that the standard $k-\epsilon$, RNG $k-\epsilon$ and Shih's nonlinear $k-\epsilon$ turbulence models have similar behavior and are close to the logarithmic law in the viscous sublayer, whereas the $k-\omega$ SST and realizable $k-\epsilon$ models agree with the logarithmic law in the viscous sublayer and extend this similarity to the transition region. Moreover, it is important to highlight that the logarithmic law theory was established for the development of the boundary layer in a Couette flow. Despite being used as a reference, the logarithmic law becomes partially representative in different geometries, such as in circular cross section pipe, and consequently, the occurrence of discrepancies is certainly to be expected. Therefore, all the turbulence models analyzed satisfactorily describe the velocity profile in the near-wall region, according to the semi-empirical law of the wall, confirming that the computational simulation setup was performed properly.

5.2 Turbulent Velocity Profile at the Bend

The flow configuration in an elbow exhibits challenging phenomena for turbulence modeling until today, such as geometry-induced adverse pressure gradients, streamline curvature, potential detachment and secondary flows (Slotnick

et al., 2014). These phenomena become pronounced as the flow at the pipe inlet sweeps through the elbow bend and, therefore, characteristic changes in the flow are developed in this region. Figure 3 presents the progression of the mean velocity profile along the curvature at different angles ϕ for the five investigated RANS turbulence models using the LES data from Röhrig *et al.* (2015) as benchmark. The position $r'/R = -1$ refers to the outer arc, while $r'/R = 1$ corresponds to the inner arc. In general, the velocity profiles resulted from the RANS turbulence models display a magnitude decrease in the near-wall velocity, a consequence of the turbulent viscosity overestimation. Nevertheless, based on the identified mean velocity profiles, the influence of the adverse pressure gradient within the inner arc is most effectively reproduced applying the realizable $k-\epsilon$ and $k-\omega$ SST turbulence models.

The standard $k-\epsilon$, Shih's nonlinear $k-\epsilon$ and RNG $k-\epsilon$ turbulence models fail to reproduce the changes in the mean velocity profile caused by the presence of the adverse pressure gradient, whose discrepancy is mostly pronounced in the mean momentum deficit region. Turbulence modeling should feature decreased turbulent viscosity in the inner arc in order to represent the presence of local acceleration. However, the results show that RANS turbulence models admittedly overestimate turbulent viscosity, as is in fact expected.

Based on the velocity components at $\phi = 90^o$, the quantitative criteria assigned by Kim *et al.* (2014) indicates that the most adequate turbulence model is the RNG $k-\epsilon$. However, this conclusion is indeed expected due to the intensification of secondary flows and anisotropy at the elbow outlet in the analyzed flow by Kim *et al.* (2014), characterized by Dean numbers exceeding 50800. These factors can be attributed to the accounting for the dissipative term in the RNG $k-\epsilon$ model formulation. Hence, it is consistent to state that the RNG $k-\epsilon$ turbulence model does not present a superior performance when reproducing the velocity profile at $\phi = 90^o$ in flows with reduced anisotropy intensity, such as for the present work's configuration with Dean number 13500.

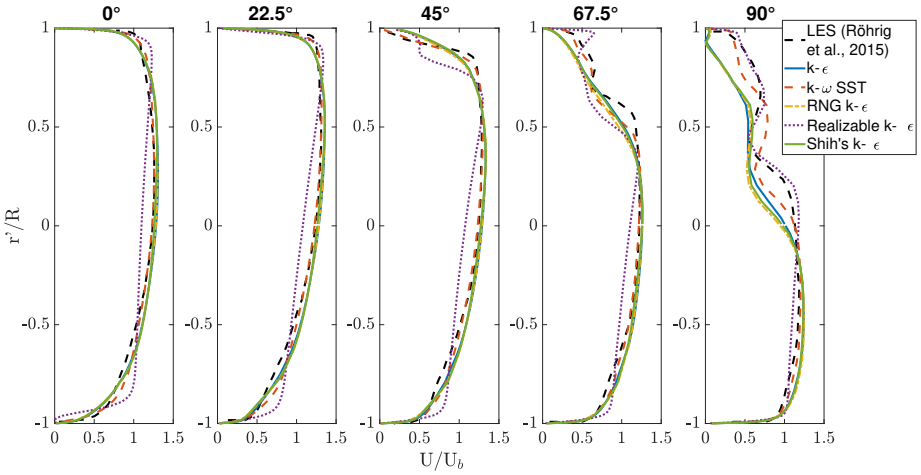

Figure 3. Evolution of the mean velocity profile within the curvature at different angles ϕ by comparing the turbulence models with LES data from Röhrig *et al.* (2015).

Furthermore, the mean velocity profiles at $z = 0.67D$ past the pipe bend for Reynolds number $Re = 24000$ were evaluated, employing the five proposed RANS turbulence models and, as a comparison, the experimental, LES, RSM and EVM standard $k-\epsilon$ data from Röhrig *et al.* (2015). From the results depicted in Fig. 4, it is initially observed that the LES data are able to fully predict the experimental velocity profile at $z = 0.67D$, in which there are low velocity magnitudes. This confirms that the LES method employed majorly solves the flow at the expense of its modeling, enabling its use as a reference in the lack of experimental data. Additionally, it evidences that, in general, the investigated turbulence models yield mean velocity profiles closer to the LES and experimental data than the reference EVM model at the inner arc. When convenient, an schematic diagram is also depicted in order to show where the referred data is being analyzed.

The results from Fig. 4 evidence that the turbulence model that provide the most accurate description of the mean velocity magnitude and thus do not overestimate the turbulent viscosity in this region is the $k-\omega$ SST model. However, although reproducing the LES results well over the whole bend, the $k-\omega$ SST turbulence model resulted in a mean velocity profile with higher disagreement with the benchmark results for $\phi = 90^o$. Particularly nearby the inner arc wall of the bend, in the region corresponding to $y^+ \leqslant 197.3$, it is observed that the velocity profile from $k-\omega$ SST model matches the behavior resulting from LES data. However, there is a change in the velocity profile, whose behavior seems to oscillate around and finally converge to the corresponding standard $k-\epsilon$ result. It is hypothesized that this might be associated with the transition applied by the blending function F_1 in the $k-\omega$ SST model, suggesting that the use of the $k-\omega$ model would supposedly reproduce the velocity profile under expressive adverse pressure gradient, whereas the deviations would be associated to the transition obtained by the blending function.

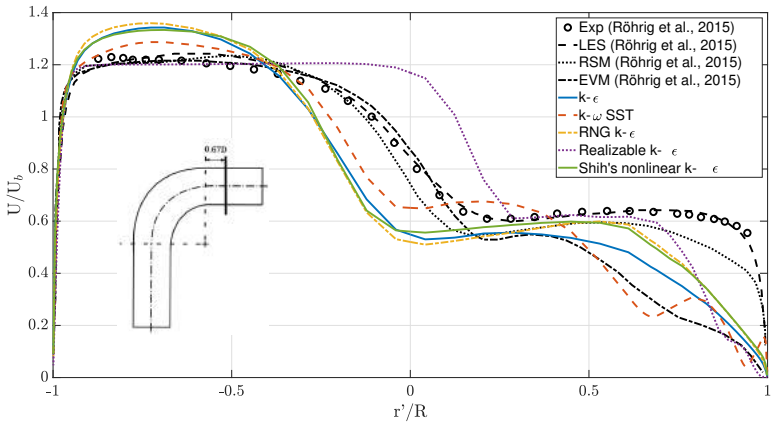

Figure 4. Comparison of the normalized mean velocity in the symmetry plane at $z = 0.67D$ between the turbulence models and experimental, LES, RSM and EVM data from Röhrig *et al.* (2015).

5.3 Analysis of the $k-\omega$ SST model blending function

Based on the results of the mean velocity profile at $\phi = 90^o$ (see for instance Fig. 3) and $z = 0.67D$ (Fig. 4) for the $k-\omega$ SST turbulence model, it was formulated a hypothesis that this model fails in this region due to the onset of the transition between the $k-\omega$ and standard $k-\epsilon$ models. In order to verify the established hypothesis, it was identified the region next to the bend inner arc at which the function F_1 is applied. It is interesting to point out that the $k-\omega$ SST turbulence model applies exclusively the $k-\omega$ model near the wall ($F_1 = 1$), transitions with corresponding $0 \leqslant F_1 \leqslant 1$ and finally, applies exclusively the standard $k-\epsilon$ turbulence model ($F_1 = 0$). Thus, the values of F_1 were computed from the turbulent kinetic energy k and specific turbulence dissipation rate ω in the wall normal direction at $z = 0.67D$, and the results are presented in Tab. 1. As a result, it was identified that the blending is applied in the y^+ interval $31.4 \leqslant y^+ \leqslant 394.5$, with a corresponding combination of the $k-\omega$ and standard $k-\epsilon$ turbulence models in this region.

Table 1. Parameters used to identify the onset and completion of the blending function F_1 application in the $k-\omega$ SST turbulence model.

y [m]	y^+	k [m^2/s^2]	ω [1/s]	F_1
9.5×10^{-4}	31.4	0.00306	689.63	0.997
1.2×10^{-2}	394.5	0.00738	215.17	0.019

From these computations, Fig. 5 shows the mean velocity profile resulting from the $k-\omega$ SST turbulence model with the identification of the start and end points of the F_1 blending function application, which marks the transition between the $k-\omega$ and $k-\epsilon$ formulations in the ascending y^+ direction. By the end of the F_1 blending function application, it is observed that the turbulence model $k-\omega$ SST predicts decreasing mean velocity magnitudes and, afterwards, tends to the velocity profile described by the standard $k-\epsilon$ model. The failure to predict the mean velocity profile possibly occurs in the region corresponding to the use of the $k-\epsilon$ formulation. Therefore, the initial hypothesis that relates the enhancement of the mismatch between the $k-\omega$ SST turbulence model and the LES data to the onset of the blending function F_1 is refuted.

5.4 Pressure and Friction Coefficients

Figure 6 shows the pressure coefficient C_p and friction coefficient C_f along the inner and outer pipe arcs, when applying the five proposed turbulence models and LES, RSM and EVM standard $k-\epsilon$ data from Röhrig *et al.* (2015). Since the pressure and friction coefficients were determined over the entire length of the bend as well as the straight duct sections, the lengths were adimensionalized, with $s < 1$ in the fluid inlet straight section, $0 < s < 1$ in the bend, and $s > 1$ in the outlet straight section. Thus, the dimensionless length $s = 0$ corresponds to the angle $\phi = 0^o$ and $s = 1$ to $\phi = 90^o$. Interestingly, the proposed turbulence models anticipate the variation of the pressure and friction coefficients in general. It is observed that the turbulence models initially predict the pressure coefficient of the flow in a similar manner to the reference data. On the other hand, the pressure coefficient prediction at the pipe outlet is closer to the LES results when applying the RNG $k-\epsilon$ turbulence model on the inner arc and the $k-\omega$ SST model on the outer arc of the pipe, which may be of particular interest in industrial applications.

Besides, through the friction coefficient, it is possible to identify the potential flow detachment from the pipe wall.

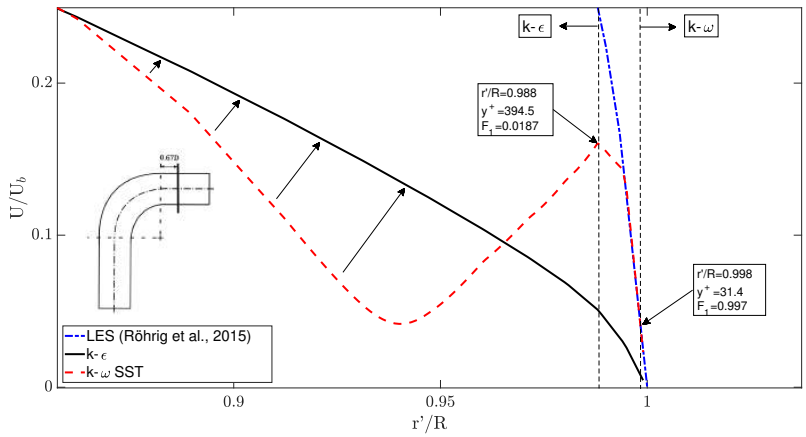

Figure 5. Normalized mean velocity in the plane of symmetry at $z = 0.67D$ resulting from LES data of Röhrig *et al.* (2015) and the application of the standard $k-\epsilon$ and $k-\omega$ SST turbulence models, which the range of application of the blending function F_1 is highlighted.

Combined with the distribution of the pressure coefficient, the behavior of the friction coefficient in LES results shows that the region with a momentum deficit reveals that the flow is close to detaching from the wall at the inner arc, as the friction coefficient approaches zero. Similar to the RSM and EVM results from Röhrig *et al.* (2015), the analyzed RANS turbulence models fail to accurately predict separation points, which are not predicted in the benchmark LES results. However, the $k-\omega$ SST and realizable $k-\epsilon$ turbulence models provide a more accurate description of the mean velocity profile at $\phi = 90^o$ due to the postponement of the flow detachment.

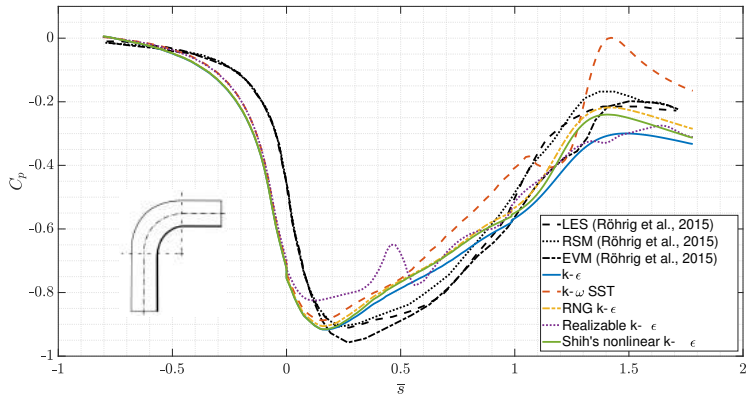

(a)

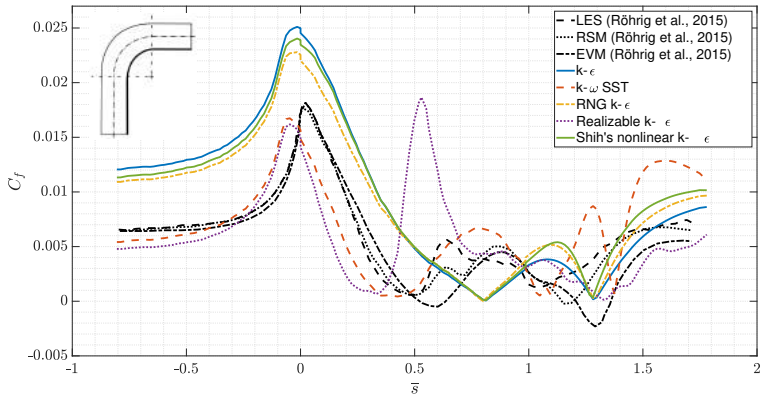

(b)

Figure 6. (a) Pressure coefficient and (b) friction coefficient along the inner arc of the pipe with normalized length by R_c at the bend for the proposed turbulence models and data from Röhrig *et al.* (2015).

5.5 Secondary Flow

As this work foresees application in multiphase flows, it is important that the prediction provided by the RANS turbulence model has greater accuracy in describing the flow velocity field, since the force characterized by the interaction between the continuous and the dispersed is given in function of the friction velocity (Sommerfeld and Laín, 2012). Accordingly, Fig. 7(a) presents the normalized mean velocity contours in the pipe cross-sections for the $k-\omega$ SST turbulence model as it describes the velocity profile more appropriately in general. The secondary flow characteristic of curved pipeline flows consist of a pair of counter-rotating cells, termed Dean vortices, which are evidenced in Fig. 7(b). According to results from Röhrig *et al.* (2015), the instantaneous velocity in the transverse planes after the pipe bends infers that Dean vortices rotate alternately clockwise and counter-clockwise. Moreover, these cells exhibit periodic oscillations similar to Von Kármán vortices (Versteeg and Malalasekera, 2007).

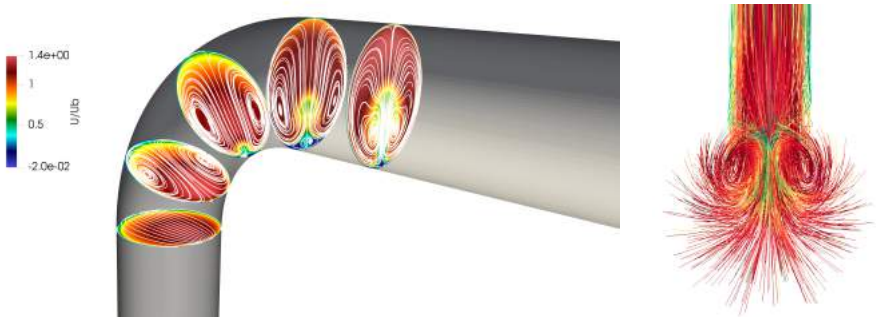

(a) (b)

Figure 7. (a) Contours of the normalized mean velocity and streamlines along the pipe applying the $k-\omega$ SST turbulence model. (b) Streamlines as they pass through the curvature highlighting the presence of Dean's vortices in frontal view.

6. CONCLUSIONS

This work compares the ability of 5 RANS turbulence models in predicting internal flow with significant streamline curvature and potential detachment region. After validating the computational setup based on the near-wall logarithmic law in the region before the bend, the performance of the turbulence models was analyzed along the bend symmetry plane and also in the region characterized by the momentum deficit. Compared to LES benchmark results, lower velocity magnitudes in the pipeline symmetry plane are associated with the Reynolds stress tensor isotropic modeling, implying overestimation of the turbulent viscosity by RANS turbulence models.

On the other hand, in the region with expressive adverse pressure gradient after the bend, the pressure coefficient is best described by the RNG $k-\epsilon$ model and none among the proposed RANS turbulence models is able to accurately predict the friction coefficient according to LES results in this region. Therefore, instead of the perspective of determining a unique and universally accurate model, it should be determined optimized turbulence models that are application-oriented and based on the relevant criteria in each case. In the presence of a favorable pressure gradient, the $k-\omega$ SST turbulence model is able to predict the results adequately compared to the other models, whereas it fails in regions with a significant adverse pressure gradient. This suggests that the failure to predict the mean velocity profile in this region occurs from the termination of the blending function F_1. Such behavior is possibly related to the majority and integral use of the standard $k-\epsilon$ model by the $k-\omega$ SST turbulence model.

Oriented for use in internal turbulent flows and the prediction of the velocity field, the results of the computational simulations indicate that in the region with streamline curvature the $k-\omega$ SST turbulence model most appropriately describes the velocity profile. Nevertheless, in the region with adverse pressure gradient the velocity profile is best described by the realizable $k-\epsilon$ turbulence model. Furthermore, the results suggest that possibly the intrinsic transient aspect of turbulence can also be an important factor alongside with anisotropy to be analyzed when describing the flow dynamics. This statement arises from the transient approach of the LES method providing significantly close results to the experimental data, while the application of Shih's $k-\epsilon$ turbulence model, which considers anisotropic effects, does not yield improvements over the other models.

7. REFERENCES

Bradshaw, P., 1987. "Turbulent secondary flows". *AnRFM*, Vol. 19, pp. 53–74.

Bredberg, J., 2000. "On the wall boundary condition for turbulence models". *Chalmers University of Technology, Department of Thermo and Fluid Dynamics. Internal Report 00/4. G oteborg*.

Breunig, J., 2017. "Which turbulence model should you use for your cfd analysis?" `https://www.xceed-eng.com/which-cfd-turbulence-model/`, Acessado em 10/05/2020.

Conde, K.E., 2018. *Geração de malhas para geometrias complexas e problemas conjuga-*

dos de transferência de calor em coletores solares híbridos aletados. Ph.D. thesis, Realização de Instituto Tecnológico de Aeronáutica. São José dos Campos: ITA. URL http://www.bdita.bibl.ita.br/tesesdigitais/lista_resumo.php?num_tese=75478. Acesso em: 4 jan. 2021.

Crawford, N., Spence, S., Simpson, A. and Cunningham, G., 2009. "A numerical investigation of the flow structures and losses for turbulent flow in 90 elbow bends". *Proceedings of the Institution of Mechanical Engineers, Part E: Journal of Process Mechanical Engineering*, Vol. 223, No. 1, pp. 27–44.

Davidson, L., 2015. "An introduction to turbulence models".

Duraisamy, K., Spalart, P.R. and Rumsey, C.L., 2017. "Status, emerging ideas and future directions of turbulence modeling research in aeronautics".

Fox, R.W., McDonald, A.T. and Mitchell, J.W., 2020. *Fox and McDonald's introduction to fluid mechanics*. John Wiley & Sons.

Greenshields, C.J., 2020. "Openfoam user guide version 8".

Jones, W. and Launder, B.E., 1972. "The prediction of laminarization with a two-equation model of turbulence". *International journal of heat and mass transfer*, Vol. 15, No. 2, pp. 301–314.

Kalpakli, A. and Örlü, R., 2013. "Turbulent pipe flow downstream a 90 pipe bend with and without superimposed swirl". *International Journal of Heat and Fluid Flow*, Vol. 41, pp. 103–111.

Kim, J., Yadav, M. and Kim, S., 2014. "Characteristics of secondary flow induced by 90-degree elbow in turbulent pipe flow". *Engineering Applications of Computational Fluid Mechanics*, Vol. 8, No. 2, pp. 229–239.

Larsson, I., Lindmark, E., Lundström, T.S. and Nathan, G., 2011. "Secondary flow in semi-circular ducts". *Journal of fluids engineering*, Vol. 133, No. 10.

Launder, B. and Spalding, D., 1974. "The numerical computation of turbulent flows". *Computer methods in applied mechanics and engineering*, Vol. 3, No. 2, pp. 269–289.

Menter, F.R., 1992. "Influence of freestream values on k-omega turbulence model predictions". *AIAA journal*, Vol. 30, No. 6, pp. 1657–1659.

Menter, F.R., Kuntz, M. and Langtry, R., 2003. "Ten years of industrial experience with the sst turbulence model". *Turbulence, heat and mass transfer*, Vol. 4, No. 1, pp. 625–632.

Moukalled, F., Mangani, L., Darwish, M. *et al.*, 2016. *The finite volume method in computational fluid dynamics*, Vol. 6. Springer.

Oberkampf, W.L. and Trucano, T.G., 2002. "Verification and validation in computational fluid dynamics". *Progress in aerospace sciences*, Vol. 38, No. 3, pp. 209–272.

Perini, F., Zha, K., Busch, S. and Reitz, R., 2017. "Comparison of linear, non-linear and generalized rng-based k-epsilon models for turbulent diesel engine flows". Technical report, SAE Technical Paper.

Pope, S.B., 2001. "Turbulent flows".

Röhrig, R., Jakirlić, S. and Tropea, C., 2015. "Comparative computational study of turbulent flow in a 90 pipe elbow". *International Journal of Heat and Fluid Flow*, Vol. 55, pp. 120–131.

Shih, T.H., Liou, W.W., Shabbir, A., Yang, Z. and Zhu, J., 1994. "A new k-epsilon eddy viscosity model for high reynolds number turbulent flows: Model development and validation". *NASA Sti/recon Technical Report N*, Vol. 95, p. 11442.

Shih, T.H., 1993. *A realizable Reynolds stress algebraic equation model*, Vol. 105993. National Aeronautics and Space Administration.

Slotnick, J., Khodadoust, A., Alonso, J., Darmofal, D., Gropp, W., Lurie, E. and Mavriplis, D., 2014. "Cfd vision 2030 study: a path to revolutionary computational aerosciences".

Sommerfeld, M. and Laín, S., 2012. "Analysis of dilute phase pneumatic conveying through pipe systems by the euler / lagrange approach".

Sudo, K., Sumida, M. and Hibara, H., 1998. "Experimental investigation on turbulent flow in a circular-sectioned 90-degree bend". *Experiments in Fluids*, Vol. 25, No. 1, pp. 42–49.

Versteeg, H.K. and Malalasekera, W., 2007. *An introduction to computational fluid dynamics: the finite volume method*. Pearson education.

White, F.M. and Corfield, I., 2006. *Viscous fluid flow*, Vol. 3. McGraw-Hill New York.

Wilcox, D.C. *et al.*, 1998. *Turbulence modeling for CFD*, Vol. 2. DCW industries La Canada, CA.

Yakhot, V., Orszag, S., Thangam, S., Gatski, T. and Speziale, C., 1992. "Development of turbulence models for shear flows by a double expansion technique". *Physics of Fluids A: Fluid Dynamics*, Vol. 4, No. 7, pp. 1510–1520.

8. RESPONSIBILITY NOTICE

The authors are solely responsible for the printed material included in this paper.